Combining Remote Sensing Techniques to Optimize Digital Surface Models for Change Detection – A Case Study at a Pit Wall in the Canadian Cordillera

Teressa Gierc, *Renato* Macciotta*, and *Fangzhou* Liu

University of Alberta, Department of Civil and Environmental Engineering, Edmonton, Canada
**Corresponding author: macciott@ualberta.ca*

ABSTRACT

Slope monitoring is vital for open pit mines during operations and nearing closure where pit wall instabilities are present. Change detection using terrestrial laser scanning (TLS) has become part of the state of practice for collecting accurate measurements with extensive spatial coverage. The approach can detect displacements associated with global slope movement, as well as surficial occurrences such as rockfalls and sloughs. However, TLS acquisition quality is vulnerable to atmospheric interference and reflectivity of the target materials. In this regard, the high-density surface information obtained from TLS could be complemented with other, less detailed, remote sensing information in order to construct a complete surface model. Such an approach, however, requires a systematic workflow and a means to calculate surface model reliability. The subject of this study is an unstable pit wall at an open pit coal mine transitioning to closure. The site is located in the Canadian Cordillera, in a setting with intermittent fog and cloud cover, wildfire haze, and seepage within the slope face and toe. Insufficient TLS data can be obtained in local areas of the slope impacted by these conditions, as well as in shadowed areas on the benches above the TLS base elevation. Aerial photogrammetry was undertaken using UAV and combined with the TLS scan to generate a representative surface model. This paper presents a methodology for registration improvement between the TLS and UAV photogrammetry clouds, and evaluation of the combined surface using concepts of Limit of Detection (LOD) adopted from change detection techniques.

Keywords: LIDAR, UAV, Change Detection, remote monitoring, rock slopes, site characterization, slope monitoring

1. Introduction

Remote monitoring methods have become common practice for slope movement monitoring at open pit mines (Macciotta and Hendry 2021; Sharon and Eberhardt 2020), allowing surveyors to remain away from bench faces where occurrences such as rockfall and raveling can occur. Conventional remote monitoring methods include terrestrial and satellite-based Interferometric Synthetic Aperture Radar (InSAR), Light Detection and Ranging (LiDAR) methods (also referred to as laser scanning), photogrammetry, and traditional total stations paired with survey monuments (Bolkas et al. 2021; Stead et al. 2019; Huntley et al. 2021).

Long range terrestrial laser scanning (TLS) is an accepted method for use in remote sensing of natural and engineered slopes (Lato, Smebye, and Kveldsvik 2017; Francioni et al. 2018; Macciotta and Hendry 2021). Notably, TLS has been successful at a number of steep rock slopes across the Canadian Cordillera (Stead et al. 2019; Lato et al. 2015; Kromer et al. 2015). The method is characterized by dense spatial coverage and high resolution and precision, which makes it desirable for change detection applications (Abellán et al. 2014). TLS requires line-of-sight clarity to produce successful data acquisition, along with ground conditions that allow for strong laser reflectivity and returns (Lato 2010). Resultantly, the quality of the TLS can be compromised when less than optimal conditions, such as wet ground and atmospheric interference.

The likelihood of collecting poor quality or insufficient data due to flawed conditions in the Canadian Cordillera is high; as such, a strategy to maximize good quality data collection is critical to produce useable data in a cost-effective manner. Combination of the TLS model with other, less accurate methods can be used to improve the topographic model of the site. The challenge is developing a systematic, repeatable, and practicable approach to develop reliable surface models for future change detection from different remote sensing techniques, and understanding the precision of the combined model. In this study, we propose a methodology for combining data collected from two acquisition methods using a procedure derived from change detection techniques. The procedure is applied for a coal mine site where the nature of the ground materials, combined with haze and fog, resulted in spatially extensive data gaps in the TLS data. Aerial photogrammetry was collected and combined with TLS data to form a complete site surface model.

The study was conducted at an open pit coal mine located in the Canadian Cordillera, close to Sparwood, British Columbia. The mine is currently on care and maintenance. Deformations of the west pit slope were identified near the completion of mining and have since been monitored by the mine, using terrestrial mobile InSAR and total stations. The post-mining displacement rate for the slope has been measured at 1 mm/day, although displacement rates have reached a maximum of 260 mm/day (Bidwell et al. 2022).

2. Methodology

2.1. Workflow

The process (Figure 1) starts with planning and completing the data acquisition on site, followed by point cloud generation, registration of point clouds, merging of a final surface model, and estimating the error associated with the monitoring technologies and merging process. These steps are detailed in this section, illustrated with the specific tools deployed for the case study. Best practices for data acquisition are summarized in Abellán et al. (2014), which are outside the scope of this paper.

In the case study that illustrates the proposed methodology, monitoring data was collected with an Optech ILRIS-LR Lidar system for TLS and with a DJI Phantom 4 Pro UAV for aerial photogrammetry. The acquisitions to be merged must be acquired concurrently to neutralize any 4D (time-dependent) changes to the slope face. This allows the user to assume that any detected difference between the two scans is a result of different acquisition technologies and compounded error.

Once collected, the raw TLS data is parsed using Optech's proprietary software, ILRIS Parser. Similarly, the UAV photographs are processed to generate a point cloud using the ADAM Technologies 3DM Mine Mapping suite (ADAM Technologies n.d.). The clouds are then imported to the point cloud processing software, CloudCompare (2023). During the cloud registration and error assessment stages, images collected using a GigaPan PanTilt terrestrial photography unit (GigaPan 2012) are used to visually assess the sources of error in each region of the slope. Using CloudCompare, the TLS and UAV photogrammetry clouds are registered in an iterative process of manual and automated fine alignment to minimize the offset between two clouds. The quality of the registration of the two point clouds is assessed using multi-scale model-to-model cloud comparison (M3C2) distance computations.

Once optimal registration is achieved, the model is assessed using an approach analogous to that of determination of the Limit of Detection (LOD) for change detection, which is derived from the compounded TLS error (Fey and Wichmann 2017; Deane et al. 2020) (further described in Section 3), using a M3C2 computation to assess the magnitude and distribution of error between the two clouds.

The aim of the error assessment is to inform the LOD calculation for future application of change detection against subsequent data sets and interpretation of change detection results by practitioners.

2.2. Data Collection

2.2.1. Site conditions

The base station for the TLS scan was situated at the south end of the opposite (east) pit wall, resulting in an oblique line of sight and excess shadows being produced in the resultant TLS point cloud. Additionally, the east side of the pit was lower in elevation than the west side, meaning that the bench surfaces could only be captured by the TLS for benches situated below the base location. For benches higher than the TLS base location, generally only the bench faces were able to be captured.

Given the availability of only one TLS scan location and the low vantage point, the decision to utilize the UAV to generate a photogrammetric point cloud was made. This would allow acquisition of data on the upper benches, as well as reduce shadows in the TLS data.

The scans were acquired on August 31, 2023. The visibility (Figure 2) was moderately clear, although there was a slight visible haze associated with wildfires in the region, as well as intermittent low clouds. No significant rainfall occurred during scanning, but heavy rainfall had occurred earlier in the day and the days prior, resulting in wet ground conditions and slope seepage.

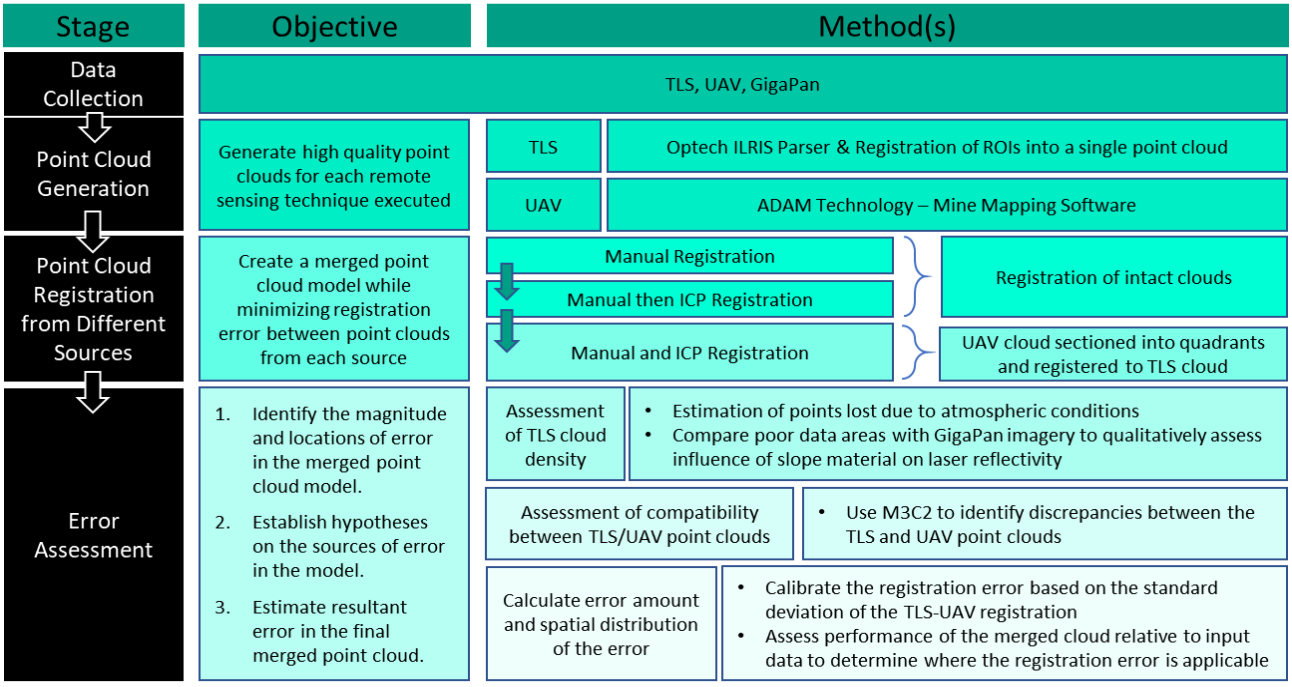

Figure 1. Study Workflow and Methodology

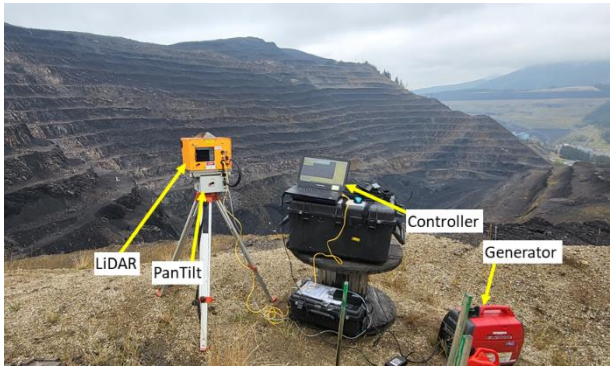

Figure 2. LTS Base Station Setup with the study area in the backdrop, looking northwest.

2.2.2. Terrestrial Laser Scan

The TLS was acquired using Optech's ILRIS-LR Laser Scanner (Optech) using the Enhanced Range mode, which is rated for a 3000 m range under optimal conditions, although this can be significantly reduced in suboptimal settings.

Given the proximity of the scan location to the slope and the 40° field of view, the scan was completed in two frames, splitting the scan into a north half and a south half. Each half was scanned in approximately 45-60 minutes, starting with the south frame and then rotating manually to the north frame. The south scan was further delineated into two regions of interest (ROIs) to account for slope/sightline geometry and varying range; the north scan was delineated into three ROIs. This is meant to keep a similar point cloud density for the entire slope surface model. The ROI locations are shown in Figure 3.

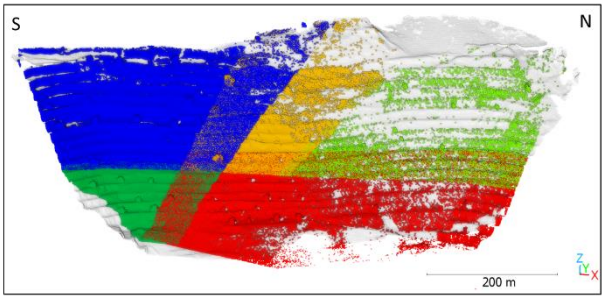

Figure 3. Study area with TLS ROIs, counterclockwise from top left corner: 101 (Blue), 102 (Dark Green), 129 (Red), 130 (Light Green), and 131 (Yellow). Untrimmed and projected atop UAV surface model (White).

2.2.3. UAV Aerial Photogrammetry

Aerial photogrammetry was obtained with a remotely piloted UAV. A DJI Phantom 4 was used to acquire the aerial photos with oblique image capturing and a manual flight path to maintain the distance between the slope and the camera as constant as possible. The angle of the photos was kept at 30 degrees from horizontal. Photogrammetry requires a set of pictures with enough overlap to reconstruct the terrain surface with a resolution that captures the slope features of interest. This can be achieved by allowing a minimum overlap of 60% between images, collecting at least three photos per feature, and using high-resolution cameras (Rodriguez et al. 2020). The UAV used in the surveys had a 12-MP camera with a sensor 1/2.3″ CMOS (6.3 mm width and 4.7 mm height), a 94° field of view, a 20 mm focal length, and an aperture of f/2.8. The internal GPS has a hovering accuracy of ± 1.5 m.

This acquisition method relies on optical imagery and line-of-sight clarity, so good lighting is required (Wollenberg-Barron et al. 2023). However, the advantage of this system is that the unit can be flown close to the slope and bypass most of the atmospheric disturbances that impede terrestrial methods (such as the TLS scan conducted concurrently). The accuracy of the aerial photogrammetry is a function of distance to the slope and pixel resolution (Küng et al. 2012; Martínez-Carricondo et al. 2018).

2.2.4. GigaPan Terrestrial Photography

Terrestrial photographs were captured using a 36.2 megapixel Nikon D800 DSLR camera fitted with a 200 mm, fixed focal length lens. The camera was mounted on a GigaPan EPIC Pro pan-tilt unit, which generates high-resolution panoramas from a grid of photographs (GigaPan 2012). The GigaPan shot ranged approximately 500 m to 750 m distance from the pit wall face.

The GigaPan is a useful photogrammetric technique which provides rapid visualization of the slope for confirmation of features identified in a point cloud model. This tool is often used to support the assessment of failure mechanisms in rock slopes along with other techniques (e.g., TLS). The GigaPan can also provide evidence of other aspects of rockfall events, such as discolouration of the slope or slickensides/scar textures which would not be visible in a point cloud model. Combining this technique with other instrumentation can provide a better understanding of the pre- and post-deformation of displacement mechanisms.

2.3. Data Processing

2.3.1. TLS Parsing & Data Cleaning

The TLS raw scan data was converted into an 8-bit xyz format (binary files) using Optech's ILRIS Parser software. Once the TLS data was parsed, the .bin files were uploaded into CloudCompare (Version 2.12.4) Open Source Software (CloudCompare 2023) for registration and analysis. Due to the erratic point density distribution of the cloud, no automated filtering of the data was used to remove outlier points or noise (which is typically done in processing TLS data), so as to avoid losing any additional data in the low-density areas. Cleaning was limited to manual trimming of the data to the extent of the study area. This was facilitated by the lack of vegetation, with the point cloud representing bare ground.

2.3.2. UAV Photogrammetry

Photographs were processed using ADAM Technology's Mine Mapping software suite. This software package builds a digital surface model based on overlapping sets of photos using photogrammetric principles on digital or scanned photographs. The software can then export the digital surfaces as raster, TINs, point clouds, etc. The process requires selecting the photographs with adequate overlap (over 60% is

recommended), removing blurry photos, and assuring full coverage of the area of interest (Rodriguez et al. 2020). With the photos selected, the software identifies common pixels for overlapping photos (manual entry is also possible). Then, the software utilizes photogrammetric principles (geometry and perspectives based on common pixel relative locations, UAV GPS stations and known ground points) to statistically calculate the location of the camera for each photo and then reconstruct the surface. The resulting point cloud had a point density of about 3.2 points per square meter (points/m^2).

2.3.3. Point Cloud Registration & Sectioning

Registration of the UAV and TLS clouds should be undertaken in a multi-stage, iterative approach.

Using the higher accuracy sourced acquisition (TLS) as a base, the photogrammetry cloud can be first scaled and aligned as a whole. Manual alignment should be used to pre-orient the clouds to reduce the number of computations required by the ICP; this requires the user to select discrete corresponding points on the base and aligned clouds, requiring visual identification of common features between the clouds. Depending on the size of the site, a minimum of 10 alignment points should be used.

Once roughly aligned, fine registration can be undertaken in CloudCompare, utilizing the automated Iterative Closest Point (ICP) algorithm developed by Chen and Medioni (1992) and Besl and McKay (1992). Depending on the distribution of error in the fine registration, it may be necessary to section the aligned cloud to address any distortion in the surface scene induced by the hardware of different acquisition systems.

2.3.4. M3C2 Processing

Once the cloud registration is optimized, an M3C2 computation is performed to assess the distribution of errors in the registration of the two clouds. M3C2 is the preferred method for cloud distance computations as it considers the normal distance between compared cloud surfaces rather than an absolute distance between adjacent points, which conventional cloud-to-cloud computations provide.

The M3C2 starts by designating "core" points – or query points – from the base cloud. These core points are locations where the M3C2 distances are computed. To generate the core points, the points surrounding each base cloud point are sampled and used to generate a representative plane in space, with the core point being at the center of that plane. A normal vector is centered at each core point (CloudCompare). In this way, surface roughness, which may be present in the model, is neutralized, giving a more realistic representation of the distance between clouds. Once the normal vector is established at each core point, a cylinder of customizable diameter is projected in both directions from the core point along the axis of the normal vector. The distance to the adjacent cloud is computed based on the average distance of the points present within the cylinder relative to the core point location. The result is reported as the M3C2 distance, generally expressed using the mean distance (μ) for all core points assessed and the standard deviation of the distances (σ).

The M3C2 computation requires a base cloud with relatively dense and uniform point cloud density for the computation of the normal vector. The UAV photogrammetry point cloud was used as the base cloud for this assessment, given the regular point distribution across the site as compared with the TLS point cloud, which contains numerous voids.

For the generation of the normal vector, all neighboring points within a selected radius of each core point are used. The radius is a function of the point density and surface roughness; insufficient point cloud density would require a larger radius for normal computation to ensure a sufficient sample size, however excessive radius will introduce error into the calculation by smoothing features out of the surface expression. Too small of a radius, conversely, prohibits determination of a normal direction due to an insufficient number of points to sample (CloudCompare). Given the point cloud characteristics, a minimum radius of 1.5 m was necessary to minimize invalid normal computations at most core points.

The cylindrical normal projection centered on the core points is used to delineate the points in the compared cloud which are used to compute the cloud-to-cloud distances. The diameter of the projection needs to be adequately sized such that the computation can detect a sufficient number of points from the compared cloud to generate a reliable M3C2 distance (CloudCompare). A projection diameter of 1.5 m was used in consideration of the cloud properties.

2.3.5. GigaPan Panorama

The terrestrial photos were merged into a high-resolution panorama using GigaPan's proprietary software, Stitch (2013). Striving for a typical 30% overlap between adjacent photos ensures any distortion between input images is minimized (Lato, Smebye, and Kveldsvik 2017). The resultant image was composed of 132 photos with a total size of 1328 megapixels.

3. Results & Discussion

3.1 TLS Cloud Density

Point cloud densities were calculated as the number of points in the trimmed cloud, divided by the surface area of the ROI. The surface area was generated from the TLS point cloud using the Poisson Surface Reconstruction plug-in in CloudCompare. The plug-in applies a triangular mesh generation algorithm by Misha Kazhdan of Johns Hopkins University (2006).

A summary of the point cloud densities by ROI is provided in Table 1, and the overall point cloud density distribution is illustrated in Figure 4a. No clear correlation is evident between the range of the scan and the point cloud density, except for a division between north and south ROIs. This suggests that the variation of point densities between ROI scans is influenced more heavily by other factors, such as atmospheric or reflectivity conditions than it is by range. There is a substantial reduction in the number of points between the raw data and the trimmed data for each ROI – especially for ROI 130, where almost 92% of the total data points

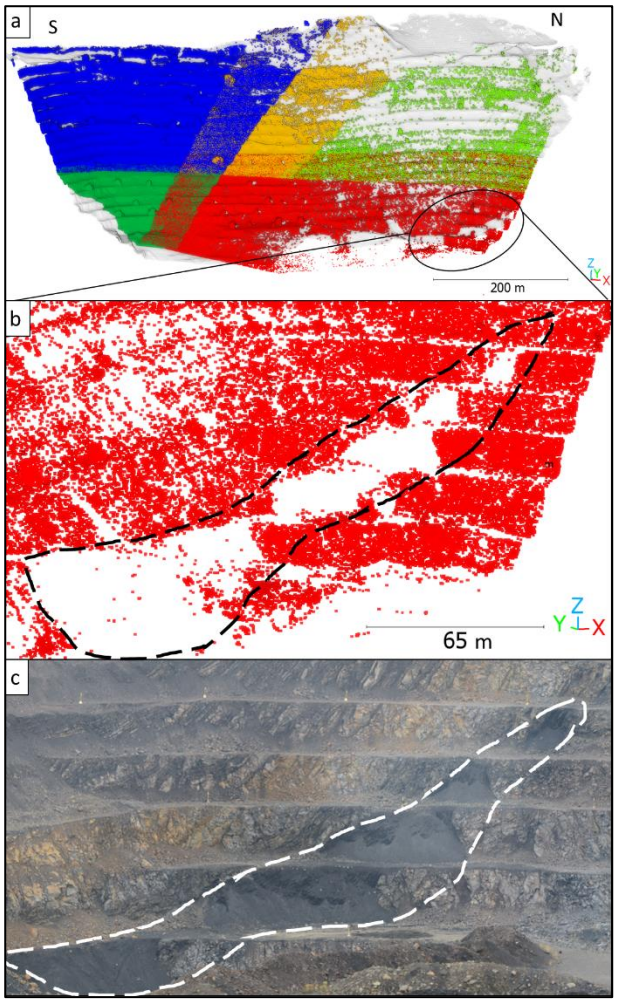

Figure 4. Local absence of laser reflectivity evident in raveled coal-rich material at a daylighting section of the coal seam. a) Coal seam location within slope area, b) TLS point cloud at coal seam location., c) GigaPan image of coal seam location (scaled approximately with image b)

collected were localized in midair between the slope surface and the equipment. This represents laser reflections caused by atmospheric issues, which is exacerbated in the long-range mode of the system (e.g. excessive moisture, suspended particles).

Slope areas void of points or with locally low point cloud density were identified and compared with the GigaPan images to qualitatively assess any trends between point density and surface material. In general, it was observed that coal-rich areas correlated with lower laser returns. Several areas of the slope characterized by sloughed or talus/ravelled coal on the benches were noted to have produced no reflections (Figure 4).

3.2 Assessment of Registration Methods

The results of the cloud registration were assessed using the M3C2 plug-in in CloudCompare. Methods assessed included 1) automated (ICP) fine registration, 2) manual registration, and 3) ICP applied to a sectioned cloud. The registration results by method are provided in Figure 5. For convention, positive values represent the TLS cloud positioned on top of the UAV points; negative values indicate the UAV cloud positioned on top.

Fine registration using the ICP method (Method 1) yielded a mean M3C2 distance of 55 mm and a standard deviation of 294 mm. Due to the inequality in point densities across the TLS cloud, this registration method introduced a registration bias. The denser half of the site was well aligned as it had a higher component of the point population, while the lower density areas exhibited large offsets between point clouds (Figure 5a).

To counter the effect of the density bias described above, manual cloud registration was used (Method 2). This approach mitigates the point density bias apparent in Method 1 as the user can evenly distribute the selection of corresponding points throughout the surface, thereby applying even weighting across the entire slope. Using manual registration achieved an M3C2 mean distance of 4 mm and a standard deviation of 191 mm (Figure 5b).

The third approach (Method 3) which was undertaken involves sectioning the point cloud into quadrants and individually registering each quadrant using ICP. This method addressed the issue of bias in the point cloud while being able to capitalize on the rapid computations available with automated ICP registration. The execution of this method took into account the transition between high- and low-density cloud areas, with each partition having relatively consistent or evenly distributed point density to avoid density bias. The resultant registration (Figure 5c) was improved to a mean M3C2 distance of -5 mm and a standard deviation of 136 mm. The final surface model was assessed based on registration Method 3 (Figure 5c).

As shown in Table 2, the overall model is generally well registered, however several areas demonstrate excess misalignment (i.e. standard deviations in excess of about 200 mm), notably the south flank and the upper north quadrant. The well-aligned areas have a mean distance of -1 mm, and a standard deviation of 117 mm.

Table 1. Summary of Point Cloud Densities for TLS ROIs

ROI ID	Range* (meters)	Number of Raw Points	Number of Points after Trimming	Approx. Surface Area (m2)	Overall Density (points/m2)
101	479 – 645	8 858 565	5 607 913	129 000	43.5
102	406 – 476	2 832 468	886 094	32 000	27.7
129	436 – 720	2 936 640	686 920	146 000	4.7
130	694 – 918	1 244 800	77 943	110 000	0.71
131	555 – 713	1 477 567	385 124	80 000	4.8

* Distance from the TLS base station to the slope face.

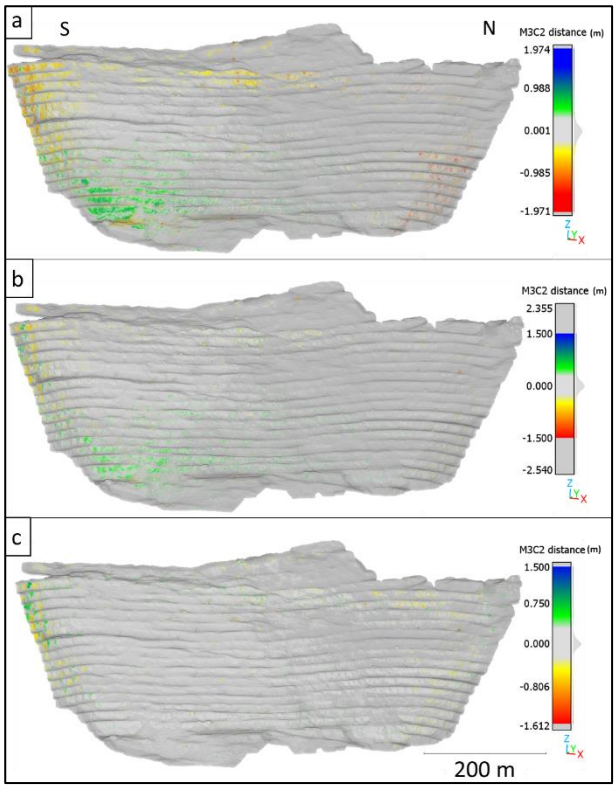

Figure 5. M3C2 Distances based on Method 1 (a), Method 2 (b), and Method 3 (c).

Table 2. Variation in Registration by Slope Area

Location	M3C2 Distance (mm)	
	Mean	**Standard Deviation**
South Flank	0	243
North Flank	-71	161
Upper North Quadrant	-36	202
Well Aligned Areas	1	117
Overall	*-5*	*136*

On the south flank, the GigaPan panorama shows the surface to have a highly notched and serrated structure (Figure 6). Given the angle of the TLS shot, depressions and notches on the slope face were poorly captured by the TLS. This is paired with the resolution of the UAV scan failing to capture the detail of the sharp protrusions and depressions of the rock, and resulting in excessive smoothing of the surface. The result is a mean M3C2 distance of zero, and a high standard deviation of 243 mm.

The upper north quadrant (central part of ROI 130) and north flank had mean M3C2 distances of -36 mm and -71 mm, respectively. Reviewing the TLS input cloud, point acquisition in these areas was poor. With insufficient TLS points, the M3C2 computation in this area becomes unreliable due to low sample size. In these areas, the merged point cloud is based primarily on the UAV photogrammetry cloud.

3.3 Core Point Positions

The performance of the merged point clouds as a complete acquisition is based on the position of the core points relative to the original input data. To assess which

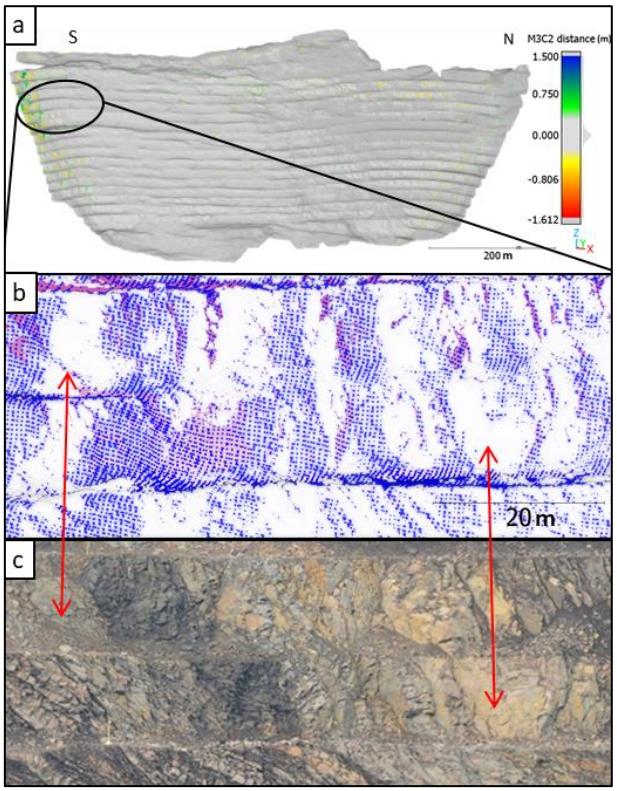

Figure 6. Sample of registration error between the point clouds. (a) Slope area, adapted from Figure 5. (b) Cloud model as viewed in CloudCompare (UAV blue, TLS white). (c) GigaPan image of slope (scaled with figure b). Red arrows indicate corresponding points between (a) and (b).

input cloud is dominant in the selection of core points in the merged model, the core points were exported as a new point cloud and compared with the input TLS and the UAV point clouds individually using M3C2.

The core points generated by the merged clouds are positioned at the weighted average point between the input cloud surfaces, noting that where only one input cloud is present, the core points represent the average surface of the singular cloud. As such, the location of the core points is dependent on the density of each cloud and the separation between them (Figure 7).

Where the TLS cloud is significantly denser than the UAV photogrammetry cloud (TLS cloud density >> 3.2 points/m^2), the core points are generated based primarily on the TLS cloud, and the error in the merged cloud is based on the accuracy of the TLS acquisition. Where the TLS cloud is absent or sparse (e.g. less than 3.2 points/m^2), the error is dependent on the UAV acquisition and/or registration.

The mean M3C2 distance calculated against the TLS input cloud is -1 mm with a standard deviation of 46 mm. In comparison, the mean distance calculated against the UAV photogrammetry cloud is 8 mm with a standard deviation of 142 mm. This corroborates that the generation of core points is primarily based on the TLS input cloud, and that the estimated registration error in the merged cloud is mostly attributable to the UAV data. This also allows us to recognize that where the TLS cloud is dense, any separation between TLS and UAV clouds has little impact on the error present in the merged model.

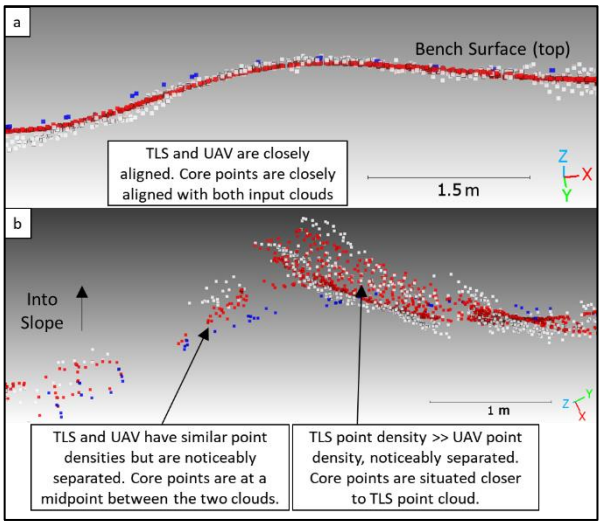

Figure 7. Examples of core point positions (red) based on input cloud (blue – UAV; white – TLS) characteristics.

3.4 Error Assessment

The goal of this study was to estimate the error compounded as a result of merging the point clouds, and to inform LOD determination for future change detection assessments of the subject slope.

The error in the final merged point cloud was evaluated using M3C2 to evaluate the separation between the two input clouds. By determining the distance between point clouds where both clouds are present, the results can be used as a calibration tool for the registration error, which can be extrapolated to estimate the error in areas where only one cloud is present.

The process used is analogous to LOD assessment for change detection using M3C2 (Deane et al. 2020; Fey and Wichmann 2017); Deane et al. (2020) considers any change calculated below two standard deviations as measurement randomness. In the context of this study, we define two standard deviations of the M3C2 distance as the error present in the merged point cloud. Pursuing this approach, the registration error for the optimized merged cloud is estimated to be a maximum of two times the standard deviation of 136 mm (Figure 5), equaling 272 mm. Extrapolating this error estimate to areas where the TLS point cloud is absent, it is expected that the inferred TLS surface would generally be within 272 mm of the UAV surface.

3.4.1. Spatial Distribution of Error

With consideration for the performance of the merged cloud outlined in Section 3.2 and the relative cloud densities outlined in Section 3.1, we consider the calculated error margin is localized to areas of the merged point cloud where the TLS point cloud density is less than or similar to that of the UAV point cloud density.

To illustrate this, the M3C2 distance results in Figure 5 are provided with distances greater than 272 mm being colourized, highlighting areas of the slope where the separation between the clouds is larger than the expected error. This condition is most prominent on the south flank, where the maximum M3C2 distance is about 1.0 m. However, given the TLS density in this area is high, the resultant core points are generated close to the TLS cloud, nullifying the fact that the separation between clouds is high.

Additional locations of excess M3C2 distance are present in the vicinity of ROI 130, where the TLS point cloud is most sparse and unable to detect local features such as boulders atop benches or the concrete bases for the monitoring prisms. These occurrences are highly localized and could be manually assessed for changes at the time of future change detection processing. Alternatively, if a higher error could be tolerated for the project applications, it may be possible to use an LOD of 500 mm in the change detection analysis to further reduces the number of highlighted areas within the slope, therefore reducing the effort in the manual assessment of those locations.

Figure 8 demonstrates the adjustments to the error estimate considering the removal of M3C2 comparison for areas with high TLS point density (namely, the south ROI areas which have point densities greater of 25 points/m^2, significantly higher than the average UAV point cloud density of about 3.2 points/m^2), and increase to the colourized limit to 500 mm.

Based on Figure 8, a change detection executed with the final merged point cloud would have an associated registration error of 0.5 m, and in turn would be capable of reliably detecting displacements greater than 0.5 m. The error is attributable primarily to the lower accuracy acquisition method (the UAV photogrammetry) and localized only to areas where the cloud composition consists primarily of the lower accuracy point cloud.

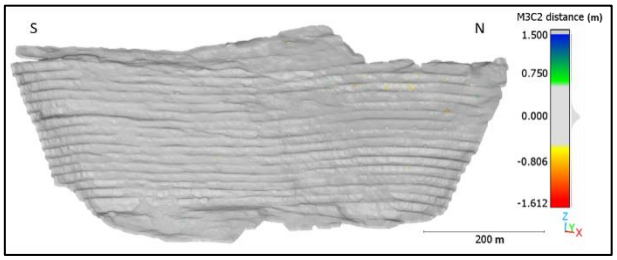

Figure 8. M3C2 results for merged clouds with significant error being shown for cloud distances in excess of 500 mm in the North ROI areas. M3C2 results nullified for the South ROIs where TLS point density >> UAV density.

4. Conclusions

TLS is an established method for site characterization which can be used effectively for change detection applications, but can be highly sensitive to adverse site conditions. In suboptimal conditions, other less accurate acquisition methods may be used to fill in local gaps in the TLS and generate a complete surface model. The registration of the merged clouds can be assessed using an M3C2 computation.

The methodology was applied in a case study of an open pit mine site using UAV and TLS acquisitions. The merging of the UAV to the TLS cloud introduced an estimated registration error of 272 mm in the regions where TLS data was poor or absent. By supplementing it with the UAV data, the TLS cloud (which was originally considered unsuitable for use) can be applied to change detection analyses for identification of instability events with a minimum thickness of 272 mm, such as rockfalls and sloughs.

Acknowledgements

The authors wish to acknowledge the mine personnel for their contributions to the work presented in this paper and for facilitating access to the subject site, as well as for providing slope monitoring data for comparison with our acquisitions. Funding for this study was provided by the Natural Sciences and Engineering Research Council of Canada (NSERC ALLRP 587029-23).

References

ADAM Technology "3DM Analyst", Available at: www.adamtech.com.au.

Abellán, Antonio, Thierry Oppikofer, Michel Jaboyedoff, Nicholas J. Rosser, Michael Lim, and Matthew J. Lato. 2014. "Terrestrial laser scanning of rock slope instabilities." *Earth Surface Processes and Landforms* 39 (1):80-97. https://doi.org/10.1002/esp.3493.

Besl, Paul J., and Neil D. McKay. 1992. "Method for registration of 3-D shapes." Proc.SPIE, 1992/4//.

Bidwell, Andrew, Olivia Wojcieszynski, James Russell, and Kate Burnham. 2022. "Considerations for GNSS Monitoring of Pit Slope Displacements." International Slope Stability 2022 Symposium, Tucson, Arizona, 2022.

Bolkas, Dimitrios, Gabriel Walton, Ryan Kromer, and Timothy Sichler. 2021. "Registration of multi-platform point clouds using edge detection for rockfall monitoring." *ISPRS Journal of Photogrammetry & Remote Sensing* 175:366-385. https://doi.org/10.1016/j.isprsjprs.2021.03.017.

Chen, Yang, and Gérard Medioni. 1992. "Object modelling by registration of multiple range images." *Image and Vision Computing* 10 (3):145-155. https://doi.org/10.1016/0262-8856(92)90066-C.

CloudCompare. "CloudCompareWiki.", [online] Available at: http://www.cloudcompare.org/doc/wiki/

"CloudCompare (version 2.12.4)", 2023. Available at: www.cloudcompare.org/

Deane, Evan, Renato Macciotta, Michael T. Hendry, Chris Gräpel, and Roger Skirrow. 2020. "Leveraging historical aerial photographs and digital photogrammetry techniques for landslide investigation-a practical perspective." *Landslides* 17 (8):1989-1996. https://doi.org/10.1007/s10346-020-01437-z.

Fey, Christine, and Volker Wichmann. 2017. "Long-range terrestrial laser scanning for geomorphological change detection in alpine terrain - handling uncertainties." *EARTH SURFACE PROCESSES AND LANDFORMS* 42 (5):789-802. https://doi.org/10.1002/esp.4022.

Francioni, Mirko, Riccardo Salvini, Doug Stead, and John Coggan. 2018. "Improvements in the integration of remote sensing and rock slope modelling." *Natural Hazards* 90 (2):975-1004. https://doi.org/10.1007/s11069-017-3116-8.

GigaPan. 2012. GigaPan EPIC Pro User Guide. GigaPan Systems. Available at: www.gigapan.com/cms/manual/pdf/epicpro-manual.pdf

GigaPan "Stitch, Version 2.1", Available at: www.gigapan.com/cms/support/download-gigapan-stitch

Huntley, David, Peter Bobrowsky, Drew Rotheram-Clarke, Roger Macleod, Robert Cocking, Jamel Joseph, Jessica Holmes, Shane Donohue, Jonathan Chambers, Phil Meldrum, Paul Wilkinson, Michael Hendry, and Renato Macciotta. 2021. "Protecting Canada's Railway Network Using Remote Sensing Technologies." In: Singhroy, V. (eds) Advances in Remote Sensing for Infrastructure Monitoring. Springer Remote Sensing/Photogrammetry. Springer, Cham., 81-109. https://doi.org/10.1007/978-3-030-59109-0_4

Kazhdan, Misha. "Poisson Surface Reconstruction", [CloudCompare plugin]. Available at: www.cloudcompare.org/doc/wiki/index.php/Poisson_Surface_Reconstruction_(plugin)

Kromer, Ryan A., D. Jean Hutchinson, Matt J. Lato, Dave Gauthier, and Thomas Edwards. 2015. "Identifying rock slope failure precursors using LiDAR for transportation corridor hazard management." *Engineering Geology* 195:93-103. https://doi.org/10.1016/j.enggeo.2015.05.012.

Küng, O., C. Strecha, A. Beyeler, J. C. Zufferey, D. Floreano, P. Fua, and F. Gervaix. 2012. "The Accuracy of Automatic Photogrammetric Techniques on Ultra-light UAV Imagery." *Int. Arch. Photogramm. Remote Sens. Spatial Inf. Sci.* XXXVIII-1/C22:125-130. https://doi.org/10.5194/isprsarchives-XXXVIII-1-C22-125-2011.

Lato, M., H. Smebye, and V. Kveldsvik. 2017. "Mapping the Inaccessible with LiDAR and Gigapixel Photography: A Case Study from Norway."

Lato, Matthew. 2010. "Geotechnical applications of LiDAR pertaining to geomechanical evaluation and hazard identification."

Lato, Matthew J., D. Jean Hutchinson, Dave Gauthier, Thomas Edwards, and Matthew Ondercin. 2015. "Comparison of airborne laser scanning, terrestrial laser scanning, and terrestrial photogrammetry for mapping differential slope change in mountainous terrain." *Canadian Geotechnical Journal* 52 (2):129-140. https://doi.org/10.1139/cgj-2014-0051.

Macciotta, Renato, and Michael T. Hendry. 2021. "Remote Sensing Applications for Landslide Monitoring and Investigation in Western Canada." *Remote Sensing* 13 (3). https://doi.org/10.3390/rs13030366.

Martínez-Carricondo, Patricio, Francisco Agüera-Vega, Fernando Carvajal-Ramírez, Francisco-Javier Mesas-Carrascosa, Alfonso García-Ferrer, and Fernando-Juan Pérez-Porras. 2018. "Assessment of UAV-photogrammetric mapping accuracy based on variation of ground control points." *International Journal of Applied Earth Observation and Geoinformation* 72:1-10. https://doi.org/10.1016/j.jag.2018.05.015.

Optech. ILRIS-LR Summary Specification Sheet. Available at: www.ticgroup.com.tw/menu/products/sur/products/3D_Laser/ILRIS%20LR.pdf

Rodriguez, J., R. Macciotta, M. T. Hendry, M. Roustaei, C. Gräpel, and R. Skirrow. 2020. "UAVs for monitoring, investigation, and mitigation design of a rock slope with multiple failure mechanisms—a case study." *Landslides* 17 (9):2027-2040. https://doi.org/10.1007/s10346-020-01416-4.

Sharon, Robert, and Erik Eberhardt. 2020. *Guidelines for Slope Performance Monitoring*: CSIRO PUBLISHING.

Stead, Doug, Davide Donati, Andrea Wolter, and Matthieu Sturzenegger. 2019. "Application of Remote Sensing to the Investigation of Rock Slopes: Experience Gained and Lessons Learned." *ISPRS International Journal of Geo-Information* 8:296-296. https://doi.org/10.3390/ijgi8070296.

Wollenberg-Barron, Taylor Del Gerhard, Renato Macciotta Pulisci, Chris Gräpel, Kristen Tappenden, and Roger Skirrow. 2023. "Comparison of Rating Systems for Alberta Rock Slopes, and Assessment of Applicability for Geotechnical Asset Management." *Geosciences* 13 (11):348. https://doi.org/10.3390/geosciences13110348